JACS
JOURNAL OF THE AMERICAN CHEMICAL SOCIETY

Article

pubs.acs.org/JACS

Subpicosecond Intersystem Crossing in Mono- and Di(organophosphine)gold(I) Naphthalene Derivatives in Solution

R. Aaron Vogt, Thomas G. Gray,* and Carlos E. Crespo-Hernández*

Department of Chemistry and Center for Chemical Dynamics, Case Western Reserve University, Cleveland, Ohio 44106, United States

Supporting Information

ABSTRACT: Femtosecond-to-microsecond broadband transient absorption experiments are reported for Cy_3PAu(2-naphthyl) (**1**), $(Cy_3PAu)_2$(2,6-naphthalenediyl) (**2**), and $(Cy_3PAu)_2$(2,7-naphthalenediyl) (**3**), where Cy = cyclohexyl. Global and target analyses of the data, based on a sequential kinetic model, reveal four spectral components. These components are assigned to (1) excited state absorption (ESA) of the ligand-centered S_1 state; (2) ESA of a receiver ligand-to-metal or metal-to-ligand charge transfer triplet state ($\tau_1 \leq 300$ fs); (3) ESA of the vibrationally excited, ligand-centered T_1 state ($\tau_3 = 7-10$ ps); and (4) ESA of the relaxed T_1 state. Intersystem crossing (ISC) occurs in hundreds of femtoseconds, while internal conversion (IC) in the triplet manifold is slow ($\tau_2 \approx 2$ ps). The relaxed T_1 state shows biphasic decay kinetics in **2** and **3** with lifetimes of hundreds of picoseconds and hundreds of nanoseconds in air-saturated conditions, while only monophasic decay is observed in **1** under identical conditions. The primary decay pathway of the T_1 state is assigned to quenching by O_2, while the secondary channel is tentatively assigned to self-quenching or triplet−triplet annihilation. The ISC rate in **1** is not modulated significantly by the incorporation of a second heavy-atom group effecter. Instead, the position at which the second Au(I)−phosphine group is attached plays a noticeable role in the ISC rate, showing a 3-fold decrease in that of **2** compared to that of **3**. The results challenge the conventional view that the rate of IC is larger than that of ISC, lending further support to the emerging kinetic model proposed for other transition-metal complexes. Gold(I) now joins the exclusive group of transition metals known to form organometallic complexes exhibiting excited-state nonequilibrium dynamics.

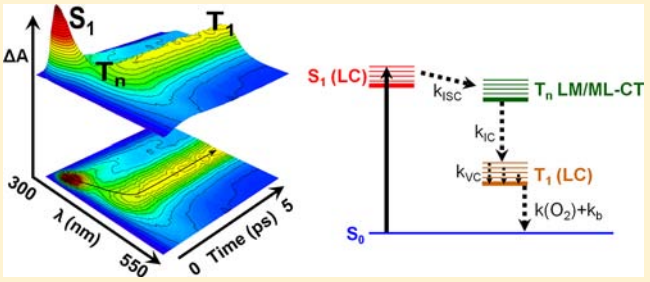

1. INTRODUCTION

The design of heteroatomic organic compounds exhibiting high triplet yields continues to attract interest because of their potential technological and life sciences applications.[1−9] In particular, the chemistry of organogold(I) compounds is receiving much attention for potential use in advanced materials in metallotherapeutic drugs, photodynamic therapy, and organic near-infrared emitter and sensor applications.[6,10−16] The formation of a gold(I)−carbon σ bond can significantly modify the electronic states of an organic aromatic compound[17−20] by enhancing spin−orbit interactions, thus increasing the rate of radiationless transition between singlet and triplet states relative to the gold(I)-free hydrocarbon counterpart.[20,21] For instance, organogold(I) compounds can exhibit dual luminescence at room temperature with emission yields that depend sensitively on the position of auration.[17,18,21−24] Most photophysical investigations performed thus far have focused on describing the absorption and emission properties of the newly synthesized gold(I) organometallics.[17−19,22,23] Much less is known, however, regarding the excited-state dynamics and relaxation mechanisms that are at play in this family of compounds.[20,21] This fundamental information is essential to current efforts aimed at tuning the photophysical properties of these novel systems and for the rational design of advanced luminescent materials based on gold(I) functionalization.[12,13,21]

In this contribution, we unravel the electronic structure and excited-state dynamics of Cy_3PAu(2-naphthyl) (**1**), $(Cy_3PAu)_2$(2,6-naphthalenediyl) (**2**), and $(Cy_3PAu)_2$(2,7-naphthalenediyl) (**3**) in dichloromethane. Contrary to the (organophosphine)gold(I)−pyrene and the oligo(*o*-/*m*-/*p*-PE)−gold(I) complexes investigated recently,[20,21,23] these gold(I)-substituted naphthalenes show remarkably large intersystem rate constants ($\sim 10^{12}-10^{13}$ s^{-1}) and unusually slow rates of internal conversion in the triplet manifold ($\sim 10^{11}$ s^{-1}). The subpicosecond intersystem crossing lifetimes measured for the gold(I) compounds in this work are among the fastest observed in transition metal complexes,[25−34] showing that auration can tune the excited-state dynamics of organic compounds to the strongly nonadiabatic regime. Importantly, we have resolved in time and in frequency the upper electronic state that acts as a doorway state in the ultrafast population of the phosphorescent state in these

Received: April 14, 2012
Published: August 21, 2012

   dx.doi.org/10.1021/ja303592q | J. Am. Chem. Soc. 2012, 134, 14808−14817

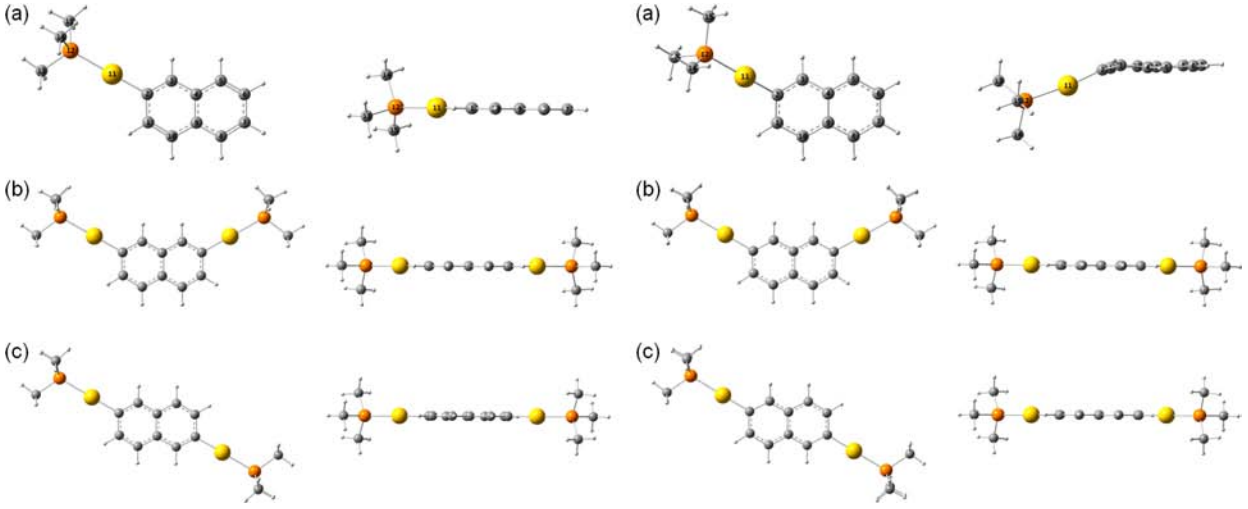

Figure 1. Optimized structures of the ground state of the model mono- and digold(I) naphthalene compounds (a) **1′**, (b) **2′**, and (c) **3′** at the PBE0/(E)-IEFPCM/LANL2DZ level of theory in dichloromethane (left panel). Optimized structures of the first excited singlet state of the model mono- and digold(I) naphthalene compounds at the TD-PBE0/(E)-IEFPCM/LANL2DZ level of theory in dichloromethane (right panel). The number assignment of atoms is shown in (a) and in higher definition in the SI. Carbon atoms are shown in gray, gold atoms in yellow, phosphorus atoms in orange, and hydrogen atoms in white. *Z*-matrices are given in the SI.

gold(I) organometallic compounds. This was achieved by using global and target analysis[35,36] based on a sequential kinetic model. To the best of our knowledge, these aurated naphthalenes represent the first examples of organogold(I) compounds exhibiting subpicosecond intersystem crossing dynamics.

2. RESULTS

Quantum Chemical Calculations. All quantum-chemical calculations for Cy_3PAu(2-naphthyl) (**1**), $(Cy_3PAu)_2$(2,6-naphthalenediyl) (**2**), and $(Cy_3PAu)_2$(2,7-naphthalenediyl) (**3**) were performed with methyl groups in place of the cyclohexyl groups on phosphorus. Hereafter, they are identified as **1′**, **2′**, and **3′**, respectively. The S_0- and S_1-optimized structures for **1′**, **2′**, and **3′** in dichloromethane are shown in Figure 1. The naphthalene moiety is planar in the S_0 state, while phosphorus has a tetrahedral geometry and a P−Au−C_2 bond angle of ∼180° in all three compounds. The S_0 geometries are in good agreement with those reported in the gas phase previously.[19] The S_1 state geometry of **1′** shows noticeable changes relative to the geometry in the S_0 state. In particular, the naphthalene moiety loses planarity, with the metalated carbon atom (C_3) going out of the plane in a semiboat-like conformation. The $C_2-C_3-C_4-C_9$ and $C_1-C_{10}-C_9-C_4$ torsion angles twist to 16.7° and −4.3°, respectively, while the P−Au−C_2 bond angle contracts by 5° relative to the bond angle of 179.9° in the S_0 geometry. In addition, the C_1-C_{10}, C_2-C_4, C_5-C_6, and C_7-C_8 bonds enlarge by 0.03 Å, while the C_1-C_2 bond contracts by the same amount relative to the corresponding S_0 bond lengths. The naphthalene moiety remains planar in the S_1-optimized structures of **2′** and **3′** (changes in torsion angles are less than 0.1°), while the C−C bonds enlarge or contract by as much as 0.06 Å relative to the S_0 bond distances. All other geometrical parameters in the S_1-optimized structures of **2′** and **3′** suffer minor changes relative to the corresponding S_0-optimized structures. The Z-matrices of the S_0- and S_1-optimized structures for **1′**, **2′**, and **3′** are given in Tables S1−S6 in the Supporting Information (SI).

The energies and oscillator strengths of the optimized S_1 states for **1′**, **2′**, and **3′** are 3.42 eV (0.0756), 3.73 eV (0.0848), and 3.66 eV (0.5018), respectively. These values were determined by using the IEFPCM equilibrium solvation model in dichloromethane. The S_1 energies are off by 0.4 eV relative to the experimental zero−zero energy of **1′** ($E_{0,0}$ = 3.88 eV) but in excellent agreement to that of **3′** ($E_{0,0}$ = 3.66 eV) in dichloromethane. For **2′**, it is not possible to estimate the zero−zero energy reliably from the absorption and fluorescence spectra (Figure 2), but the calculated S_1 energy is in excellent agreement with the lowest-energy fluorescence maximum in dichloromethane. Table 1 presents the calculated vertical excitation energies and oscillator strengths of the five and six

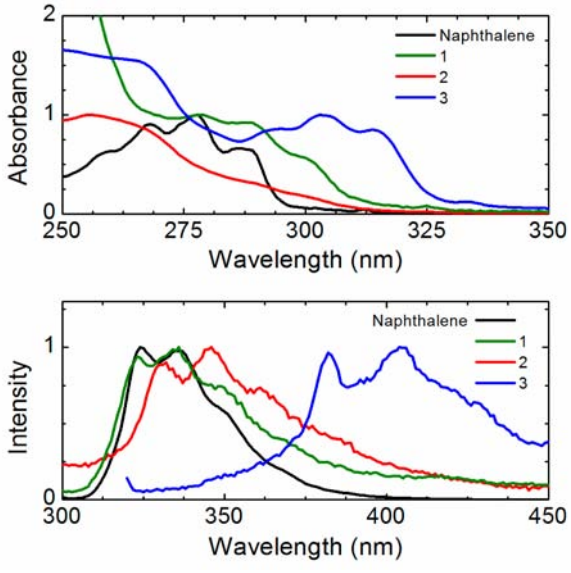

Figure 2. Comparison of the normalized absorption (top panel) and fluorescence (bottom panel) spectra of naphthalene with those for Cy_3PAu(2-naphthyl) (**1**), $(Cy_3PAu)_2$(2,6-naphthalenediyl) (**2**), and $(Cy_3PAu)_2$(2,7-naphthalenediyl) (**3**) in dichloromethane.

dx.doi.org/10.1021/ja303592q | J. Am. Chem. Soc. 2012, 134, 14808−14817

Table 1. Vertical Excitation Energies Calculated Using TD-PBE0 Functional, the LANL2DZ Basis Set, and the NE-IEFPCM Solvation Model[a]

model system	1′	2′	3′
S_1	4.37 (0.086)	4.28 (0.025)	4.20 (0.301)
S_2	4.45 (0.012)	4.28 (0.004)	4.30 (0.014)
S_3	4.63 (0.008)	4.58 (0.013)	4.59 (0.000)
S_4	5.17 (0.001)	4.82 (1.533)	4.88 (0.028)
S_5	5.19 (1.098)	4.87 (0.000)	4.90 (0.000)
T_1	2.59	2.56	2.55
T_2	3.92	3.80	3.83
T_3	4.15	4.12	4.09
T_4	4.23	4.15	4.10
T_5	4.36	4.22	4.32
T_6	4.41	4.33	4.32
$\Delta(S_1 - T_n)^b$	0.01	0.06	0.10
$\Delta(T_n - T_1)^b$	1.77	1.66	1.55
dipole moment, S_0 (D)	9.399	8.422	0.010
dipole moment, S_1 (D)	9.372	8.532	0.075

[a]These energies were obtained relative to the S_0-optimized geometry, which was optimized using the E-IEFPCM solvation model at the same level of theory. The estimated accuracy in energy from a comparison with the experimental data in Figure 2 is ±(0.2−0.3) eV. [b]T_n is the triplet state, the energy of which is closest to but lower than that of the S_1 state.

lowest-energy singlet and triplet states, respectively, for **1′**, **2′**, and **3′** in dichloromethane calculated at the optimized S_0 geometry. These vertical excitation energies and oscillator strengths were obtained by using the nonequilibrium IEFPCM solvation model, as explained in the Methods section. The S_1 vertical excitation energies are in reasonable agreement (within 0.2−0.3 eV) with the onset of the absorption spectra of each compound in the same solvent (Figure 2). The estimated accuracy of the vertical excitation energies is in very good agreement with that recently reported by Jacquemin et al.[37] for the same level of theory from a benchmark work that includes the experimental absorption and emission data of 40 compounds. In addition, there are five triplet states lower in energy than the S_1 state of **1′** and **2′**, while there are four triplet states below the S_1 state of **3′** when the S_0-optimized structures are used to calculate the vertical excitation energies. The energy gap between the S_1 state and the nearest lowest-energy triplet state in **1′**, **2′**, and **3′** is 0.01, 0.06, and 0.10 eV, respectively, when using the S_0-optimized geometry as reference. The small S_1−T_n energy gaps and the high phosphorescence yields[19] suggest the presence of strong spin−orbit coupling interactions between the singlet and the triplet manifolds in **1′**, **2′**, and **3′** in dichloromethane. Finally, and for completeness, Table 1 also includes the dipole moments of **1′**, **2′**, and **3′** in the S_0 and S_1 states in dichloromethane.

Table 2 reports the estimated percentage composition of the vertical singlet and triplet excited states calculated at the S_0-optimized geometry (see also Tables S7−S9 in SI). The principal Kohn−Sham orbital configurations are presented in the SI for each compound. We remark that a quantitative assignment of the various transitions that leads to a particular character of the excited states is difficult. To make the discussion of the excited states more straightforward, we describe each state by using the Kohn−Sham orbital configurations that play the preponderant role in the single-particle electronic transitions describing each excited state. In particular, we distinguish three types of transitions:[38,39] (1) transitions between Kohn−Sham orbitals primarily localized on the metal or metal-centered (MC) transitions; (2) transitions between Kohn−Sham orbitals primarily localized on the ligand, known as ligand-centered (LC) transitions; and (3) transitions between a Kohn−Sham orbital primarily localized on the ligand and a Kohn−Sham orbital primarily localized on the metal. The latter transitions can originate from single-particle ligand-to-metal or metal-to-ligand transitions. Therefore, they are labeled as ligand-to-metal (LM) or metal-to-ligand (ML) charge transfer transitions, LMCT or MLCT, respectively.[38,39]

Since the experimental and theoretical evidence accumulated in this and in a previous work[19] suggests that strong spin−orbit coupling between the excited electronic states is at play, it may be inappropriate to distinguish between singlet and triplet excited states in these compounds. For convenience, and as it is customary in the literature,[38] we use the spin state to label the excited states even when its denotation is not strict. In support of this choice, we note that the absorption and emission spectra of **1**, **2**, and **3** strongly resemble those of naphthalene in the same solvent (Figure 2), indicating a large LC character of the electronic transitions in these compounds and, in particular, of the S_1 states. This choice is also supported by the analysis of the character of the excited states reported in Table 2. In addition, we note that the calculations suggest that the T_1 state has mostly LC character, which is in line with the high phosphorescence yield measured for these metalated naphthalenes in solution.[19] The primary LC nature of the electronic transitions in **1′**, **2′**, and **3′** is in agreement with the LC character reported for the electronic transitions of (organophosphine)gold(I)−pyrene and oligo(*o*-/*m*-/*p*-PE)−gold(I) complexes recently.[20,21,23]

Broadband Transient Absorption Experiments. Time-resolved absorption spectra were recorded to probe the excited-state dynamics of the gold(I)−naphthalene derivatives and to reveal the decay pathways leading to the population of the phosphorescent state. Transient absorption spectra at selected time delays are given in Figure 3 for compounds **1**, **2**, and **3**, respectively. Contour plots showing the multidimensional transient absorption data are shown in Figure 4. Following

Table 2. Estimated Character of the Excited States, in Percentages, Obtained from a Time-Dependent Density-Functional Analysis of the Single-Particle Transitions Constituting Each State, Relative to the S_0-Optimized Structures (see SI for details)

model system	S_1	T_1	T_2	T_3	T_4	T_5	T_6
1′-S_0	90% LC	85% LC	86% LC	44% LC	5% LC	87% MLCT	4% LC
	10% LMCT	15% LMCT	14% LMCT	56% LMCT	95% LMCT	13% LMCT	96% LMCT
2′-S_0	90% LC	90% LC	10% LC	80% LC	50% LC	30% LC	22% LC
	10% LMCT	10% LMCT	90% LMCT	20% LMCT	50% LMCT	70% LMCT	88% MLCT
3′-S_0	80% LC	90% LC	90% LC	70% LC	30% LC	20% LC	10% MC
	20% LMCT	10% LMCT	10% LMCT	30% LMCT	70% LMCT	80% LMCT	90% MLCT

dx.doi.org/10.1021/ja303592q | J. Am. Chem. Soc. 2012, 134, 14808−14817

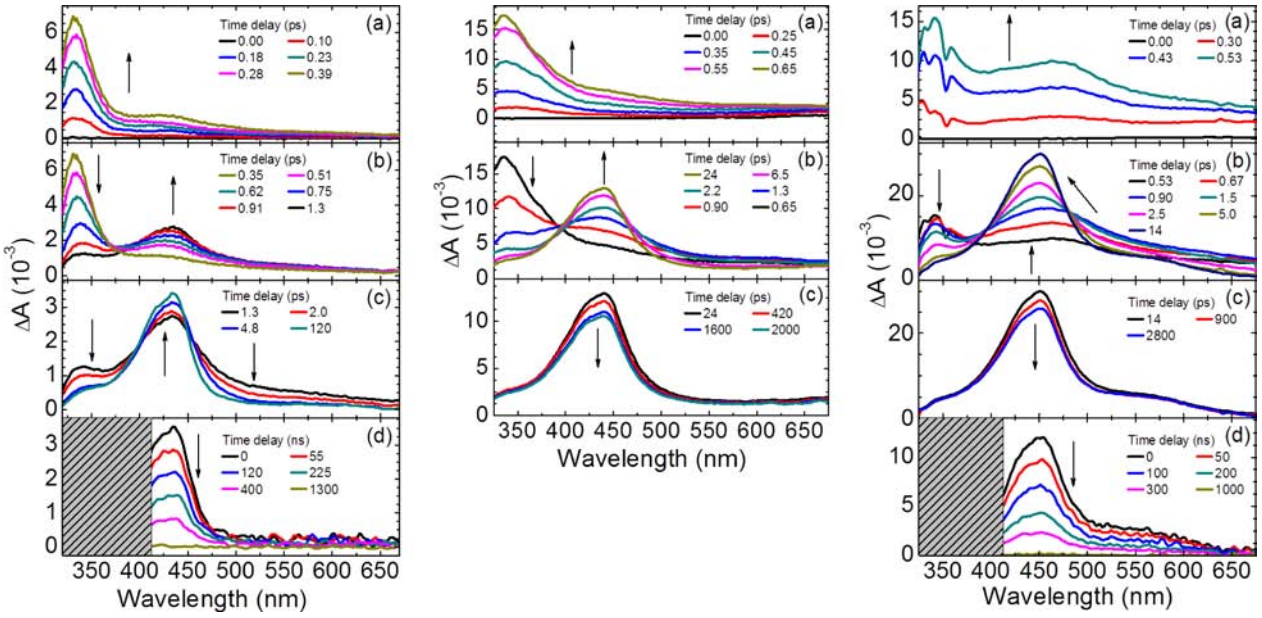

Figure 3. Two-dimensional transient absorption spectra at selected time delays for $Cy_3PAu(2\text{-naphthyl})$ (**1**) in dichloromethane excited at 285 nm (left panel); for $(Cy_3PAu)_2(2,6\text{-naphthalenediyl})$ (**2**) in dichloromethane excited at 266 nm (middle panel); and for $(Cy_3PAu)_2(2,7\text{-naphthalenediyl})$ (**3**) in dichloromethane excited at 320 nm (right panel). Stimulated Raman emission bands of the solvent are observed around 350 nm within the pulse width of the femtosecond excitation beam in graph (a) of the right panel. Graphs (c) in the left and right panels are blocked with dashed rectangles because the absolute magnitude of the absorption intensities in the spectral region below 420 nm are underestimated by the white-light generation source used in this work to probe the kinetics from the nanosecond-to-microsecond time scale.

excitation, a broad absorption band grows within the cross-correlation of the pump and probe pulses, with absorption maximum at ∼335 nm for compounds **1** and **2** and below 330 nm for **3**. We denote this absorption band as band **A** hereafter. As band **A** grows, another absorption band (band **B**, hereafter) begins to grow with maximum at 430 nm in **1**, ∼440 nm in **2**, and 470 nm in **3** (Figure 3, panel a). Band **B** continues to grow as band **A** decays (Figure 3, panel b). Figure 3 also shows that band **B** evolves within the first 2 ps to populate an absorption band in the same spectral region (band **C***, hereafter). Band **C*** blue-shifts, narrows, and becomes more structured as time progresses developing into band **C** after a few tens of picoseconds. Band **C** partially decays within a time delay of 3 ns in **2** and **3** (but not in **1**), as shown in panel c in Figure 3.

Transient absorption experiments were also performed in the nanosecond-to-microsecond time scale for compounds **1** and **3** to quantify the rate of decay of the absorption band **C** in air-saturated conditions (panel d in Figure 3). Analogous experiments for **2** were unsuccessful because of the significant degradation of this compound during the time required to collect the time-resolved data from the nanosecond-to-microsecond time window. The absorption band **C** in **1** and **3** decays monoexponentially in the nanosecond-to-microsecond time scale and, within the sensitivity of our spectrometer, no other absorption bands are observed after ∼1 μs. Transient absorption experiments performed for **1** and **3** under N_2-saturated conditions display a significant slowdown in the decay of this absorption band (data not shown), showing that this long-lived species is quenched by molecular oxygen.

Representative decay traces are shown in Figure 5 for **1**, **2**, and **3** at select probe wavelengths together with best global-fit curves. We used a global and target analysis method based on a sequential kinetic model to extract the lifetimes and decay-associated spectra from the multidimensional time-resolved absorption data. Data analysis shows that four lifetimes are needed to fit adequately the decay traces during the first 3 ns. These lifetimes are reported in Table 3, while the corresponding decay-associated spectra are shown in Figure 6. Representative decay traces for **1** and **3** in the nanosecond-to-microsecond time window, together with best global-fit curves, are shown in Figure 7. The latter decay traces were fit independently from the femtosecond-to-nanosecond transient data by using an exponential decay function convoluted with a Gaussian response function, as described in the Methods section.

3. DISCUSSION

The chief aim of this work is to unravel and to understand the electronic energy relaxation pathways that ultimately lead to phosphorescence emission in high yields in **1**, **2**, and **3** at room temperature.[19] Understanding the relaxation mechanisms that control the efficiency of triplet state population is critical to the goal of rationally synthesizing gold(I) organometallic compounds for their potential use in a wide range of applications. We begin the discussion by assigning the transient species observed in the femtosecond-to-microsecond time scale. We then present a detailed kinetic mechanism that satisfactorily explains the electronic relaxation pathways in these organometallic compounds, followed by a comparison of their excited-state dynamics with those previously reported for the (pyrenyl)gold(I)− and NO_2−naphthalene/pyrene analogues. Finally, the central results are summarized in the Conclusion.

Assignment of the Transient Absorption Bands. The time-resolved experiments reveal that five relaxation processes take place from the femtosecond-to-microsecond time scale for **2** and **3**, and four relaxation pathways for **1** (Table 3). On the basis of the accuracy of the calculated vertical excitation energies and the corresponding oscillator strengths, the S_1 states in **1**, **2**, and **3** are each assigned as the optically populated state with the pump energy used to excite each compound. We

dx.doi.org/10.1021/ja303592q | J. Am. Chem. Soc. 2012, 134, 14808−14817

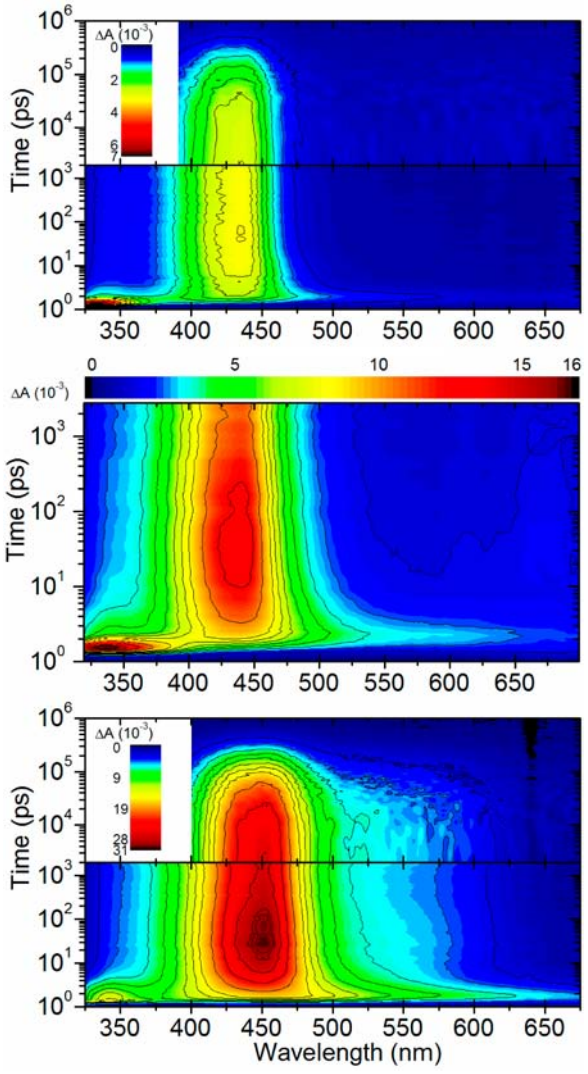

Figure 4. Top to bottom: contour representation of the multidimensional time-resolved absorption data for Cy_3PAu(2-naphthyl) (**1**), $(Cy_3PAu)_2$(2,6-naphthalenediyl) (**2**), and $(Cy_3PAu)_2$(2,7-naphthalenediyl) (**3**) in dichloromethane. Note that the time scale expands from femtosecond to microsecond in **1** and **3**, while the femtosecond scale is only expanded to the nanosecond in **2**. The transient spectra below 420 nm are blocked for **1** and **3** from the nanosecond-to-microsecond time scale (see the caption for Figure 3 for details).

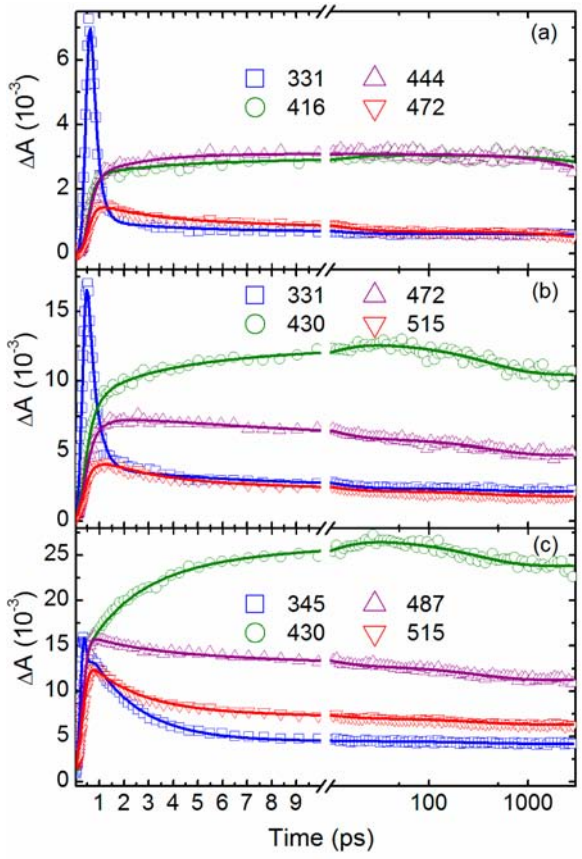

Figure 5. Representative decay traces from the femtosecond-to-nanosecond time scale for (a) Cy_3PAu(2-naphthyl) (**1**), (b) $(Cy_3PAu)_2$(2,6-naphthalenediyl) (**2**), and (c) $(Cy_3PAu)_2$(2,7-naphthalenediyl) (**3**) in dichloromethane. Best global-fit curves obtained by modeling the transient absorption data using target analysis based on a sequential kinetic model are shown by solid lines.

Table 3. Lifetimes Obtained from a Global and Target Analysis of the Transient Absorption Data Based on a Sequential Kinetic Model (τ_1–τ_4) or from an Exponential Decaying Function (τ_5); Both Model Functions Were Convoluted with the Corresponding Instrument Response Functions

	compound		
lifetime	**1**	**2**	**3**
τ_1 (fs)	~230	~330	~100
τ_2 (ps)	2.0 ± 0.5[a]	2.0 ± 0.5[a]	2.0 ± 0.5
τ_3 (ps)	10 ± 1	7.2 ± 0.8	7.6 ± 0.5
τ_4 (ps)	∞[b]	410 ± 60	310 ± 40
τ_5 (ns)	265 ± 40	–	180 ± 40

[a]Fixed to the lifetime value obtained for **3** during the global analysis. [b]This lifetime does not decay within the 3.2 ns time window and should be associated to τ_5.

note that excitation of **2** at 266 nm can, in principle, populate the three lowest-energy singlet states (Table 1). However, the magnitudes of the oscillation strengths for these states show that the S_1 state should be populated with 60% more probability than either the S_2 or S_3 states. More importantly, the striking resemblance of the early transient absorption bands and dynamics for **1**, **2**, and **3** lends further support that the S_1 state is the state being probed in Figure 3 within the time resolution of our setup in these compounds. Hence, the absorption band **A** is assigned to excited state absorption of the optically populated S_1 state. The absence of stimulated emission in the transient absorption spectra of **1**, **2**, and **3** suggests that the majority of the S_1 state dynamics is occurring on a faster time scale than that accessible using our setup.

The population in the S_1 state decays in the subpicosecond time scale (τ_1) to populate the transient species **B**. We assign this transient absorption band to a receiver triplet state (T_n) in each compound. This assignment is supported by the following experimental and computational observations. The fluorescence quantum yields of these compounds are negligible (~≤10^{-4}; see Table S10 in SI), in line with the subpicosecond lifetime (τ_1), while most of the emission yields in these compounds at room temperature are due to phosphorescence from the T_1 state.[19] In addition, the population transfer from **A** to **B** shows an isosbestic point in the transient absorption spectra of each

dx.doi.org/10.1021/ja303592q | J. Am. Chem. Soc. 2012, 134, 14808–14817

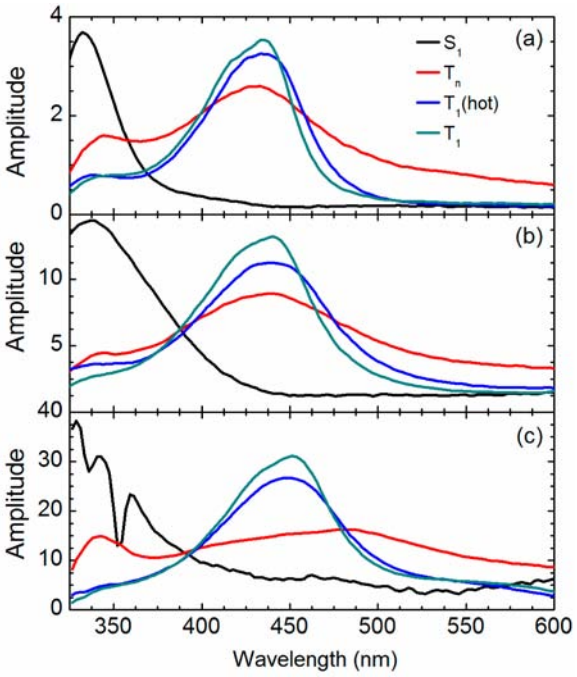

Figure 6. Decay-associated spectra of the S_1 state, the receiver T_n state, the vibrationally excited T_1 state, and the vibrationally relaxed T_1 state in (a) $Cy_3PAu(2\text{-naphthyl})$ (**1**), (b) $(Cy_3PAu)_2(2,6\text{-naphthalenediyl})$ (**2**), and (c) $(Cy_3PAu)_2(2,7\text{-naphthalenediyl})$ (**3**) in dichloromethane. The decay-associated spectra were obtained by modeling the transient absorption data using target analysis based on a sequential kinetic model. Stimulated Raman emission bands of the solvent are captured in the decay-associated spectra of the S_1 state in (c) ~350 nm in part because the dynamics of the S_1 state occurs within the pulse width of the femtosecond excitation beam. The decay-associated spectra for the S_1 state were scaled by a factor of 0.25, 0.5, and 1 for panels a, b, and c, respectively.

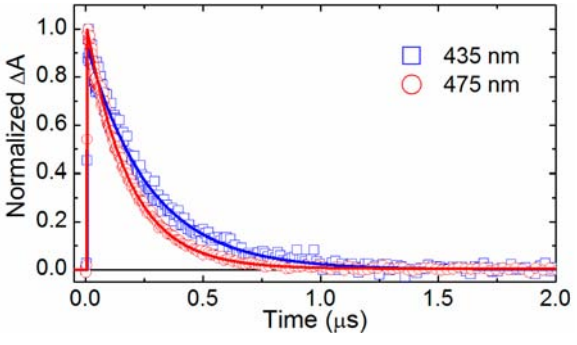

Figure 7. Representative decay traces from the nanosecond-to-microsecond time scale for $Cy_3PAu(2\text{-naphthyl})$ (**1**) (open squares) and $(Cy_3PAu)_2(2,7\text{-naphthalenediyl})$ (**3**) (open circles) in dichloromethane. Best global-fit curves obtained by modeling the transient absorption data using an exponential function convoluted with an instrument response function of 500 ps are shown by solid lines.

compound (Figure 3), which suggests state-to-state relaxation dynamics. Furthermore, the calculations predict that several upper triplet (T_n) states lie lower in energy than the S_1 state, one of which is nearly isoenergetic to the S_1 state in each compound. Specifically, the vertical excitation energies shown in Table 1 suggest the T_5 state as the receiver state in **1′** and **2′**, while it is the T_4 state in **3′**. The observation that intersystem crossing occurs in hundreds of femtoseconds suggests that singlet-to-triplet population transfer competes with intramolecular vibrational relaxation in the S_1 state (i.e., intersystem crossing probably occurs in the nonadiabatic regime).[25,28,29,34] The ultrafast nature of the intersystem crossing pathway lends support to the idea that the T_5 state is the receiver state in **1′** and **2′**, while it is T_4 state in **3′**. We remark, however, that high-level *ab initio* calculations that include nonadiabatic molecular dynamics simulations and determination of the spin−orbit overlap integrals for the intersystem crossing pathways are needed to assign unequivocally the receiver triplet state in each compound. Regardless of which upper triplet state actually serves as the doorway state, the experimental and computational evidence provides strong support for its involvement in the ultrafast intersystem crossing relaxation pathway in each compound.

The receiver T_n state (band **B**) decays in ~2 ps (τ_2) to populate the transient absorption species labeled as **C***. As shown in Figure 8, the absorption band **C*** narrows, blue-shifts,

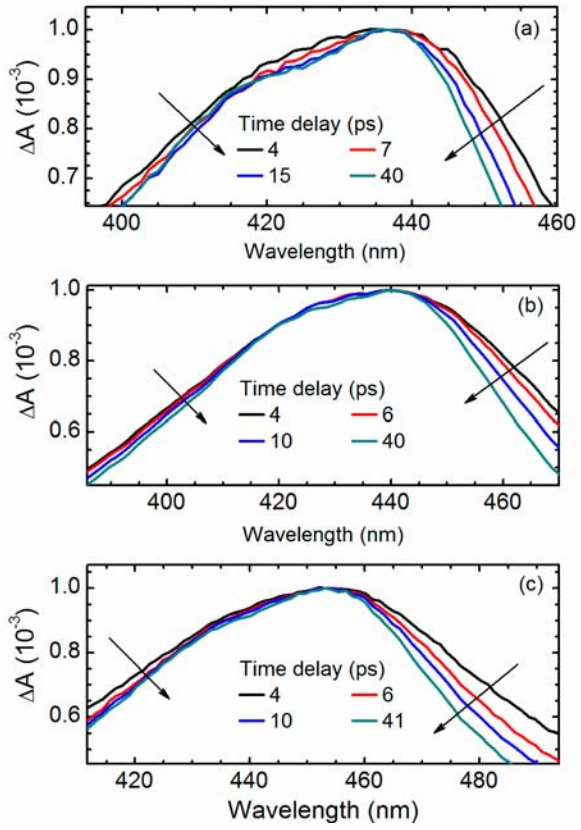

Figure 8. Normalized transient absorption spectra for (a) $Cy_3PAu(2\text{-naphthyl})$ (**1**), (b) $(Cy_3PAu)_2(2,6\text{-naphthalenediyl})$ (**2**), and (c) $(Cy_3PAu)_2(2,7\text{-naphthalenediyl})$ (**3**) in dichloromethane showing the narrowing, blue-shifting, and increased structuring characteristic of vibrational cooling dynamics.

and becomes more structured with an increase in time delay (τ_3), resulting in the formation of the long-lived absorption band **C**. Band narrowing, structuring, and blue-shifting are often hallmarks of vibrational cooling dynamics occurring in electronic states.[43−45] Consequently, we assign the decay pathway associated with the conversion of band **B** to **C*** as internal conversion in the triplet manifold (see below), while the transient species **C*** is assigned to the vibrationally excited T_1 state. The vibrationally excited T_1 state decays in 8−10 ps to

dx.doi.org/10.1021/ja303592q | J. Am. Chem. Soc. 2012, 134, 14808−14817

populate the relaxed T_1 state (band **C**). The significantly faster vibrational cooling dynamics in **2** and **3** relative to that in **1** can be understood in terms of the additional vibrational degrees of freedom provided by the second (phosphine)gold(I) group in **2** and **3**. We note that slow internal conversion and vibrational cooling dynamics in the triplet manifold have been reported previously in other naphthalene derivatives.[48−51] In this respect, the strong ligand-to-metal charge transfer character of the upper excited triplet states reported in Table 2 for **1′**, **2′**, and **3′** does not affect significantly the rates of internal conversion and vibrational cooling observed previously in other substituted naphthalene compounds. However, the covalent incorporation of (phosphine)gold(I) groups to the naphthalene framework increases the rate of intersystem crossing from the singlet to the triplet manifold.

Evidence that the band **C** should be assigned to the T_1 state comes from the observation that this transient species is quenched by molecular oxygen in the nanosecond-to-microsecond time scale. Further support for this assignment comes from the observation of high phosphorescence yield in these aurated naphthalenes at room temperature in solution.[19] Our time-resolved experiments also show that a small fraction of the population in the T_1 state decays with a lifetime of hundreds of picoseconds (τ_4) in **2** and **3** but not in **1**. This decay pathway is tentatively assigned to triplet−triplet annihilation or self-quenching, but it was not investigated further because its overall contribution to the relaxation mechanism is small. A major fraction of the T_1 state population decays in hundreds of nanoseconds in air-saturated conditions, following a pseudo-first-order rate constant characterized by $(\tau_5)^{-1}$.

The Nature of the Femtosecond Intersystem Crossing Pathway. In this section we invoke Fermi's golden rule[52] to rationalize the ultrafast nature of the rate of intersystem crossing in these gold(I)−naphthalene compounds. If we initially assume that any difference between the Franck−Condon overlap factors between the S_1 and T_n states in these compounds can be ignored, the subpicosecond nature of the intersystem crossing relaxation pathway can be qualitatively explained by the small energy gap between the S_1 and T_n states and by a presumably strong spin−orbit interaction in the region of potential energy surfaces (PES) where the population transfer occurs. Previous studies have shown that the relative magnitude of the intersystem crossing rate in other transition metal compounds correlates with the *square* of the spin−orbit integral of the intersystem crossing pathway, but not with the spin−orbit constant of the heavy metal itself.[40,41]

Interestingly, the intersystem crossing pathway in **1** is not modulated significantly by the addition of a second (phosphine)gold(I) functional group (i.e., in **1** vs **2**). This observation suggests that the magnitude of the spin−orbit interaction between the S_1 and T_n PES may be strong enough in **1** that the addition of a secondary heavy-atom group effecter no longer affects the intersystem crossing rate in **2** to a significant extent. This idea is in agreement with the above statement that it is the strength of the square of the spin−orbit integral and not the spin−orbit constant of the metal itself that plays a primary role in the magnitude of the intersystem crossing rate.

On the other hand, the observation that the intersystem crossing lifetime in **2** is approximately 3-fold less than in **3** suggests that either the magnitude of the Franck−Condon overlap factors or that of the spin−orbit integrals between the S_1 and T_n states (or both) is smaller in **2** than in **3**. Unfortunately, we cannot make any conclusions with the data on hand about which of these two factors plays a major role or if, in fact, both are equally important in controlling the intersystem crossing rate. Regardless, the position to which the second (phosphine)gold(I) group is attached, which itself might reflect a change in the Franck−Condon overlap factor, seems to modulate the intersystem crossing rate in these compounds. Thus, we suggest that changes in the topology of the PES in the vicinity where the avoided crossing between the S_1 and the T_n adiabatic PES occurs should alter the intersystem crossing rate in **2** and **3**. Clearly, information about the topology of the PES involved in the intersystem crossing relaxation pathways as well as the strength of the spin−orbit interaction that promotes them is necessary before a more quantitative discussion is warranted. Taken together, however, the above observations support the idea that intersystem crossing occurs between nonequilibrated excited states,[28,29,31,32,34,42] where the ability of active vibrational modes in the S_1 state to couple and explore the singlet−triplet crossing region might control the intersystem crossing rate.

Evidence Supporting the Slow Rate of Internal Conversion in the Triplet Manifold. The suggestion above that internal conversion in the triplet manifold is anomalously slow deserves additional discussion. The calculations presented in Table 1 show that there is a large energy difference between the T_n and T_1 states (>1.5 eV) in these three compounds. We argue that the large energy gap results in poor Franck−Condon overlap factors for internal conversion, which can explain the slow rate of internal conversion in these compounds, as expected from the energy gap law for radiationless transitions.[46,47] Furthermore, the decay-associated spectrum of the T_n state in Figure 6 is noticeably different from the T_1(hot) and T_1 spectra. This provides additional support to the idea that two different excited triplet states are probed. The slow internal conversion pathway in the triplet manifold is the reason we are able to resolve in time and frequency the receiver T_n state from the T_1 state in these gold(I)−naphthalene compounds.

Further evidence for the slow rate of internal conversion is obtained from the analysis of the transient absorption data. For instance, efforts were made in the case of **1** for using a kinetic model that has two sequential steps instead of three. However, the two-step kinetic model did not adequately fit the transient absorption data (see Figure S1 in SI), showing that a three-step sequential model is the simplest that can be used to satisfactorily model the excited-state dynamics in **1** from the femtosecond-to-nanosecond time window. Similarly, a four-step sequential model is needed to satisfactorily fit the transient absorption data for **2** and **3** in the same time window. In addition, as noted earlier, slow (ps) internal conversion in the triplet manifold has been reported in other naphthalene derivatives previously,[48−51] which makes naphthalene a unique chromophore in this respect. Altogether, the experimental and computational data available provide strong support for the proposed slow internal conversion process in the triplet manifold of these molecules. In the next section, we summarize the overall kinetic model that best explains the transient absorption data from the femtosecond-to-microsecond time scale in the gold(I)−naphthalene compounds.

Sequential Kinetic Model. Scheme 1 shows a kinetic mechanism that satisfactorily explains the excited-state dynamics observed in these organogold(I) naphthyls. This sequential model is summarized as follows. Excitation of **1**, **2**,

Scheme 1. Proposed Sequential Kinetic Mechanism Explaining the Excited-State Dynamics in Cy_3PAu(2-Naphthyl) (1), $(Cy_3PAu)_2$(2,6-Naphthalenediyl) (2), and $(Cy_3PAu)_2$(2,7-Naphthalenediyl) (3) in Dichloromethane[a]

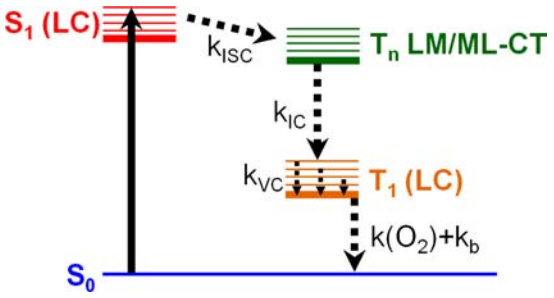

[a]Intersystem crossing from the ligand-centered S_1 state to a receiver, high-energy T_n state with ligand-to-metal (in **2′** and **3′**) or metal-to-ligand (in **1′**) charge transfer character occurs with a rate constant $k_{ISC} \approx 10^{12}-10^{13}$ s^{-1}. Intersystem crossing possibly occurs in the strong nonadiabatic regime. The doorway T_n state internally converts with a rate constant $k_{IC} \approx 5 \times 10^{11}$ s^{-1} to populate the vibrationally-excited T_1 state. Vibrational cooling dynamics in the T_1 state occurs with a rate constant of $k_{VC} \approx 1 \times 10^{11}$ s^{-1}. Finally the T_1 state decays by two parallel bimolecular relaxation pathways. The major relaxation pathway is assigned to triplet quenching by molecular oxygen, $k(O_2)$, while the second, minor channel is tentatively assigned to triplet−triplet annihilation or self-quenching (k_b).

and **3** at 285, 320, and 266 nm, respectively, populates primarily the ligand-centered S_1 state. The S_1 state intersystem crosses to populate a receiver triplet state (T_n) in hundreds of femtoseconds. The T_n state has a strong ligand-to-metal (in **2′** and **3′**) or metal-to-ligand (in **1′**) charge transfer character and internally converts to populate the vibrationally excited T_1 state in ∼2 ps. The hot T_1 state cools down to populate the relaxed T_1 state in 7−10 ps. The decay-associated spectra of these transient species are reported in Figure 6. Finally, the T_1 state decays by two parallel relaxation pathways to repopulate the ground state in **2** and **3**, but only one decay pathway is observed in **1** for the triplet state. The major relaxation pathway is assigned to quenching of the T_1 state by molecular oxygen, while the other minor channel, only observed in **2** and **3**, is tentatively assigned to self-quenching or triplet−triplet annihilation. We note that triplet−triplet annihilation has been shown to play a role in the deactivation mechanism of oligo(PE) gold(I) complexes.[21]

Comparison with (Pyrenyl)gold(I)- and NO_2-Substituted Compounds. It is instructive to compare briefly the excited-state dynamics previously reported in aurated pyrenyl derivatives[20] with those in the naphthalene-based systems presented in this work. When the naphthyl in **1** is replaced by a pyrenyl moiety, the excited-state dynamics are noticeably affected. The population of the receiver triplet state in **1** is approximately 500-fold faster than in the aurated pyrenyl derivative (pyrenyl compound labeled **2** in ref 20). In addition, internal conversion in the triplet manifold of the aurated pyrenyl compound is ultrafast, as expected, while in aurated naphthalenes internal conversion occurs in ∼2 ps. Furthermore, while the T_1 state is populated with excess vibrational energy in each of the aurated naphthalene derivatives, vibrational cooling dynamics are not observed in the (pyrenyl)gold(I) derivatives.[20]

Interestingly, the above observations echo those previously reported for 1-nitropyrene (1NP)[53] and 1-nitronaphthalene (1NN)[50] compounds. As in **1**, **2**, and **3**, 1NN shows subpicosecond population of the triplet manifold and a vibrational cooling lifetime of ∼10 ps,[50] whereas 1NP shows a slower intersystem crossing to the triplet manifold and no evidence of vibrational cooling dynamics in the T_1 state,[53] as in the (pyrenyl)gold(I) compounds.[20] Taken together, the experimental and computational evidence available thus far suggests that the excited-state dynamics of Au(I)- and NO_2-substituted naphthalene and pyrene compounds are primarily controlled by the strength of the spin−orbit interaction between the S_1 and T_n PES in the vicinity of the avoided crossing, the position in which the functional group is covalently linked (which itself might reflect a change in the Franck−Condon overlap factors and topology of the PES), as well as by how the energy and ordering of the excited states in the Franck−Condon region in the polycyclic aromatic compound are perturbed by the addition of the functional group. It will be interesting to verify if these observations can be generalized in polycyclic aromatic compounds substituted with other functional groups or with other transition metals. Such systematic experiments have the potential to increase our understanding and ultimately our control of the electronic and nuclear factors affecting the rate of intersystem crossing in organometallic compounds, currently being sought for a wide range of biological and technological applications.

4. CONCLUSIONS

The electronic structure and excited-state dynamics of Cy_3PAu(2-naphthyl), $(Cy_3PAu)_2$(2,6-naphthalenediyl), and $(Cy_3PAu)_2$(2,7-naphthalenediyl) in dichloromethane are presented. We have resolved in time and in frequency the spectral signatures of the S_1, T_n, T_1(hot), and T_1(relaxed) states by using global and target analysis based on a sequential kinetic model. It is shown that intersystem crossing to the triplet manifold occurs in hundreds of femtoseconds, presumably from the nonequilibrated S_1 state. The negligible $\Delta E(S_1 - T_n)$ energy gap and strength of the spin−orbit coupling interaction between the S_1 and the T_n PES in the region of the avoided crossing are proposed to explain the ultrafast singlet to triplet population transfer in these gold(I)−naphthalene compounds. Significantly, these aurated naphthalene compounds represent the first examples of gold(I) organometallic compounds exhibiting subpicosecond intersystem crossing dynamics, thus, expanding the group of transition metals known to promote excited-state dynamics in the strongly nonadiabatic regime. As proposed initially by McCusker and co-workers for other organometallics,[25,28,29,34] our results challenge the view that the rate of internal conversion is larger than that of intersystem crossing, hence lending further support to the kinetic model proposed in other transition-metal complexes.[25,32,34] The results presented in this work are expected to facilitate the rational design of the next generation of gold(I)-substituted organometallic monomers and oligomers with increased potential for applications as metallotherapeutic drugs, photodynamic therapy, organic near-infrared emitters, and sensing.[6,10−13]

5. EXPERIMENTAL AND COMPUTATIONAL METHODS

Broadband Transient Absorption Spectrometer. The transient absorption spectrometer used in this work has been described in detail previously.[8,50] Briefly, the output of a Quantronix Integra-i/e 3.5 Laser (100 fs centered at 800 nm) is fed into an optical parametric amplifier (OPA, TOPAS, Quantronix/Light Conversion) generating

dx.doi.org/10.1021/ja303592q | J. Am. Chem. Soc. 2012, 134, 14808−14817

the 266, 285, and 320 nm excitation pulses. Contributions from other wavelengths are removed by a reflective wavelength filter and a Glan-Taylor prism. Data are acquired using a broadband transient absorption spectrometer (Helios, Ultrafast Systems, LLC) with homemade LabView 8.6 software (National Instruments, Inc.). A continuously moving 2 mm CaF_2 crystal is used for continuum generation giving access to the spectral range from ~320 to 700 nm. The white-light probe pulses are corrected for group velocity dispersion.[50,54] The instrument response function of our experimental setup was estimated to be (250 ± 100) fs by using the coherent signal of solvent only (methanol) scans. The concentrations used for compounds **1**, **2**, and **3** in these experiments were, respectively, 4.4×10^{-4}, 1.1×10^{-4}, and 1.6×10^{-4} M. Compounds **1**, **2**, and **3** were excited at 285, 266, and 320 nm, respectively.

Data analysis was performed using Igor Pro 6.12A software (Wavemetrics, Inc.). Nineteen decay traces were selected from the multidimensional data set for each compound at equidistant probe wavelengths and analyzed using a global fitting subroutine set up in the Igor Pro software. The global and target analysis method,[35,36] based on a sequential kinetic model,[55] was used to obtain the excited-state lifetimes and decay-associated spectra of the three naphthalene derivatives studied in this work. The sequential model rate law was composed of four exponential components.[55] This function was convoluted with a Gaussian-shaped instrument response function. In the case of **1**, the lifetime of the fourth component does not decay within the 3.2 ns time window of our setup, and it is denoted by $\tau_4 = \infty$ in Table 3. Its decay is likely associated to τ_5 in Table 3. The reported uncertainties for the lifetimes shown in Table 3 are twice the standard deviation (2σ) obtained from the global analysis of three independent sets of experiments for each compound.

Transient absorption spectra of compounds **1** and **3** were also recorded from the picosecond-to-microsecond time scale using a photonic crystal fiber for probe light generation in the spectral range from ~400 to 675 nm (Eos, Ultrafast Systems, LLC). In this mode, a diode that monitors the light source is used as an external trigger that synchronizes the femtosecond system. The light source is coupled to our femtosecond transient absorption spectrometer,[50] allowing the use of the same setup for probing the excited-state dynamics from the picosecond-to-microsecond time scale. The concentrations of **1** and **3** used in these experiments were $(4.8 \pm 0.5) \times 10^{-4}$ and $(3.9 \pm 0.9) \times 10^{-4}$ M, respectively. Analogous experiments for **2** were impractical because it significantly degrades during the time required to collect the data (~5−10 min) at the excitation intensity used (see below). Data acquisition was performed using homemade LabView 8.6 software. As for the femtosecond experiments, 19 decay traces were selected from the multidimensional data set for each compound at equidistant probe wavelengths and analyzed using a global fitting subroutine set up in the Igor Pro software. The fitting subroutine consisted of an exponential decay function convoluted with a Gaussian-shaped response function of 400 ps.

The probed volume of each sample was continuously renewed using a Teflon-coated stir bar and a magnetic stirrer during all the transient absorption experiments performed in this work. The optical path length of the cell was 0.2 cm. The degradation of the compounds was monitored by using UV absorption spectroscopy, and solutions were replaced by fresh ones if the steady-state absorbance at the excitation wavelength decreased by more than 5% during the course of the experiments. The excitation intensity used in all the transient absorption experiments was 2 μJ or less.

Ground- and Excited-State Quantum Chemical Calculations. All quantum-chemical calculations for Cy_3PAu(2-naphthyl) (**1**), $(Cy_3PAu)_2$(2,6-naphthalenediyl) (**2**), and $(Cy_3PAu)_2$(2,7-naphthalenediyl) (**3**) were performed with methyl groups in place of the cyclohexyl groups on phosphorus. They were performed to assist in the interpretation of the experimental data. Ground- and excited-state calculations were performed using the Gaussian09 suite of programs.[56] The ground-state geometries were optimized at the density functional level of theory (DFT) without imposed symmetry by using the parameter-free PBE0 functional[57] and the LANL2DZ[58] basis set. The optimized ground-state structures were verified to be local minima on the PES by confirming that all vibrational frequencies have real values. Vertical and adiabatic excitation energies were calculated by using the time-dependent implementation of DFT with the PBE0 functional[57] and the LANL2DZ[58] basis set. Solvent effects were modeled by using the polarizable continuum model (PCM)[59] with the integral equation formalism (IEFPCM).[60] The equilibrium solvation model (E-IEFPCM) was used for all the calculations, except for the vertical excitation energies that used the nonequilibrium model (NE-IEFPCM). The nonequilibrium solvation model was used in the latter calculations because the aim in obtaining those vertical excitation energies was to determine the triplet state that acts as a doorway state in the subpicosecond singlet−triplet population transfer. Solvation dynamics in the excited states typically occur in similar or slower time scales in other naphthalene derivatives.[50]

■ ASSOCIATED CONTENT

Supporting Information

Z-matrices of the S_0- and S_1-optimized structures (Tables S1−S6); method used to determine the percentage of single-particle transitions contribution to the character of the vertical excited states (Tables S7−S9); principal Kohn−Sham orbitals; estimation of fluorescence and phosphorescence quantum yields (Table S10); and comparison of analysis of the transient absorption data using a two-step versus a three-step sequential kinetic model for compound **1** (Figure S1). This material is available free of charge via the Internet at http://pubs.acs.org.

■ AUTHOR INFORMATION

Corresponding Author

tgray@case.edu; carlos.crespo@case.edu

Notes

The authors declare no competing financial interest.

■ ACKNOWLEDGMENTS

C.E.C.-H. and R.A.V. thank the donors of the American Chemical Society Petroleum Research Fund for support of this work. C.E.C.-H. also thanks the Mississippi Center for Supercomputer Research, and the Ohio Supercomputer Center for generous allotment of computer time. T.G.G. acknowledges the support of the National Science Foundation (Grant CHE-1057659). We also thank Dr. Lei Gao for synthesizing and purifying the compounds.

■ REFERENCES

(1) Celli, J. P.; Spring, B. Q.; Rizvi, I.; Evans, C. L.; Samkoe, K. S.; Verma, S.; Pogue, B. W.; Hasan, T. *Chem. Rev.* **2010**, *110*, 2795−2838.

(2) Mroz, P.; Tegos, G. P.; Gali, H.; Wharton, T.; Sarna, T.; Hamblin, M. R. *Photochem. Photobiol. Sci.* **2007**, *6*, 1139−1149.

(3) Duncan, T. V.; Frail, P. R.; Miloradovic, I. R.; Therien, M. J. *J. Phys. Chem. B* **2010**, *114*, 14696−14702.

(4) Tsuboyama, A.; Okada, S.; Ueno, K. Highly Efficient Red-Phosphorescent Iridium Complexes. In *Highly Efficient OLEDs with Phosphorescent Materials*; Yersin, H., Ed.; Wiley-VCH Verlag GmbH & Co.: Weinheim, 2008; pp 163−183.

(5) Segura Carretero, A.; Salinas Castillo, A.; Fernández Gutiérrez, A. *Crit. Rev. Anal. Chem.* **2005**, *35*, 3−14.

(6) Allendorf, M. D.; Bauer, C. A.; Bhakta, R. K.; Houk, R. J. T. *Chem. Soc. Rev.* **2009**, *38*, 1330−1352.

(7) Reichardt, C.; Crespo-Hernández, C. E. *J. Phys. Chem. Lett.* **2010**, *1*, 2239−2243.

(8) Reichardt, C.; Guo, C.; Crespo-Hernández, C. E. *J. Phys. Chem. B* **2011**, *115*, 3263−3270.

(9) Reichardt, C.; Crespo-Hernández, C. E. *Chem. Commun.* **2010**, *46*, 5963−5965.

(10) Ho, S. Y.; Tiekink, E. R. T. In *Metallotherapeutic Drugs and Metal-Based Diagnostic Agents: The Use of Metals in Medicine*; Gielen, M., Tiekink, E. R. T., Eds.; Wiley: New York, 2005; pp 507−528.
(11) Partyka, D. V.; Zeller, M.; Hunter, A. D.; Gray, T. G. *Angew. Chem., Int. Ed.* **2006**, *45*, 8188−8191.
(12) Lima, J. C.; Rodríguez, L. *Chem. Soc. Rev.* **2011**, *40*, 5442−5456.
(13) Raubenheimer, H. G.; Schmidbaur, H. *Organometallics* **2012**, *31*, 2507−2522.
(14) Craig, S.; Gao, L.; Lee, I.; Gray, T.; Berdis, A. J. *J. Med. Chem.* **2012**, *55*, 2437−2451.
(15) Partyka, D. V.; Teets, T. S.; Zeller, M.; Updegraff, J. B., III; Hunter, A. D.; Gray, T. G. *Chem.—Eur. J.* **2012**, *18*, 2100−2112.
(16) Gao, L.; Niedzwiecki, D. S.; Deligonul, N.; Zeller, M.; Hunter, A. D.; Gray, T. G. *Chem.—Eur. J.* **2012**, *18*, 6316−6327.
(17) Partyka, D. V.; Esswein, A. J.; Zeller, M.; Hunter, A. D.; Gray, T. G. *Organometallics* **2007**, *26*, 3279−3282.
(18) Heng, W. Y.; Hu, J.; Yip, J. H. K. *Organometallics* **2007**, *26*, 6760−6768.
(19) Gao, L.; Peay, M. A.; Partyka, D. V.; Updegraff, J. B., III; Teets, T. S.; Esswein, A. J.; Zeller, M.; Hunter, A. D.; Gray, T. G. *Organometallics* **2009**, *28*, 5669−5681.
(20) Vogt, R. A.; Peay, M. A.; Gray, T. G.; Crespo-Hernández, C. E. *J. Phys. Chem. Lett.* **2010**, *1*, 1205−1211.
(21) Lu, W.; Kwok, W.-M.; Ma, C.; Chan, C. T.-L.; Zhu, M.-X.; Che, C.-M. *J. Am. Chem. Soc.* **2011**, *133*, 14120−14135.
(22) Gao, L.; Partyka, D. V.; Updegraff, J. B., III; Deligonul, N.; Gray, T. G. *Eur. J. Inorg. Chem.* **2009**, 2711−2719.
(23) Chao, H.-Y.; Lu, W.; Li, Y.; Chan, M. C. W.; Che, C.-M.; Cheung, K.-K.; Zhu, N. *J. Am. Chem. Soc.* **2002**, *124*, 14696−14706.
(24) Peay, M. A.; Heckler, J. E.; Deligonul, N.; Gray, T. G. *Organometallics* **2011**, *30*, 5071−5074.
(25) Damrauer, N. H.; Cerullo, G.; Yeh, A.; Boussie, T. R.; Shank, C. V.; McCusker, J. K. *Science* **1997**, *275*, 54−57.
(26) Bhasikuttan, A. C.; Suzuki, M.; Nakashima, S.; Okada, A. *J. Am. Chem. Soc.* **2002**, *124*, 8398−8405.
(27) Busby, M.; Matousek, P.; Towrie, M.; Vlček, A., Jr. *J. Phys. Chem. A* **2005**, *109*, 3000−3008.
(28) Gawelda, W.; Cannizzo, A.; Pham, V.-T.; van Mourik, F.; Bressler, C.; Chergui, M. *J. Am. Chem. Soc.* **2007**, *129*, 8199−8206.
(29) Cannizzo, A.; Blanco-Rodríguez, A. M.; El Nahhas, A.; Šebera, J.; Záliš, S.; Vlček, A., Jr.; Chergui, M. *J. Am. Chem. Soc.* **2008**, *130*, 8967−8974.
(30) Ramakrishna, G.; Goodson, T., III; Rogers-Haley, J. E.; Cooper, T. M.; McLean, D. G.; Urbas, A. *J. Phys. Chem. C* **2009**, *113*, 1060−1066.
(31) El Nahhas, A.; Cannizzo, A.; van Mourik, F.; Blanco-Rodríguez, A. M.; Záliš, S.; Vlček, A., Jr.; Chergui, M. *J. Phys. Chem. A* **2010**, *114*, 6361−6369.
(32) Juban, E. A.; McCusker, J. K. *J. Am. Chem. Soc.* **2005**, *127*, 6857−6865.
(33) Bhasikuttan, A. C.; Okada, T. *J. Phys. Chem. B* **2004**, *108*, 12629−12632.
(34) Monat, J. E.; McCusker, J. K. *J. Am. Chem. Soc.* **2000**, *122*, 4092−4097.
(35) van Stokkum, I. H. M.; Larsen, D. S.; van Grondelle, R. *Biochim. Biophys. Acta* **2004**, *1657*, 82−104.
(36) van Stokkum, I. H. M.; Larsen, D. S.; van Grondelle, R. *Biochim. Biophys. Acta* **2004**, *1658*, 262.
(37) Jacquemin, D.; Planchat, A.; Adamo, C.; Mannucci, B. *J. Chem. Comput.* **2012**, *8*, 2359−2372.
(38) Balzani, V. Photophysics of Transition Metal Complexes in Solution. In *CRC Handbook of Photochemistry*, 3rd ed.; Taylor and Francis Group, LLC: Boca Raton, 2006; pp 60−82.
(39) McMillan, D. R. In *Physical Methods in Bioinorganic Chemistry*; Que, L. Q. J., Ed.; University Science Books: Sausalito, CA, 2000.
(40) Abedin-Siddique, Z.; Yamamoto, Y.; Ohno, T.; Nozaki, K. *Inorg. Chem.* **2003**, *42*, 6366−6378.
(41) Abedin-Siddique, Z.; Yamamoto, Y.; Ohno, T.; Nozaki, K. *Inorg. Chem.* **2004**, *43*, 663−673.
(42) Cannizzo, A.; van Mourik, F.; Gawelda, W.; Zgrablic, G.; Bressler, C.; Chergui, M. *Angew. Chem., Int. Ed.* **2006**, *45*, 3174−3176.
(43) Elsaesser, T.; Kaiser, W. *Annu. Rev. Phys. Chem.* **1991**, *42*, 83−107.
(44) Owrutsky, J. C.; Raftery, D.; Hochstrasser, R. M. *Annu. Rev. Phys. Chem.* **1994**, *45*, 519−555.
(45) Nibbering, E. T. J.; Elsaesser, T. *Chem. Rev.* **2004**, *104*, 1887−1914.
(46) Englman, R.; Jortner, J. *Mol. Phys.* **1970**, *18*, 145−164.
(47) Freed, K. F.; Jortner, J. *J. Chem. Phys.* **1970**, *52*, 6272−6291.
(48) Sakamoto, M.; Cai, X.; Hara, M.; Fujitsuka, M.; Majima, T. *J. Am. Chem. Soc.* **2004**, *126*, 9709−9714.
(49) Sakamoto, M.; Cai, X.; Hara, M.; Fujitsuka, M.; Majima, T. *J. Phys. Chem. A* **2005**, *109*, 4657−4661.
(50) Reichardt, C.; Vogt, R. A.; Crespo-Hernández, C. E. *J. Chem. Phys.* **2009**, *131*, 224518.
(51) Zugazagoitia, J. S.; Collado-Fregoso, E.; Plaza-Medina, E. F.; Peon, J. *J. Phys. Chem. A* **2009**, *113*, 805−810.
(52) Turro, N. J.; Ramamurthy, V.; Scaiano, J. C. In *Modern Molecular Photochemistry of Organic Molecules*; University Science Books: Sausalito, CA, 2010.
(53) Crespo-Hernández, C. E.; Burdzinski, G.; Arce, R. *J. Phys. Chem. A* **2008**, *112*, 6313−6319.
(54) Nakayama, T.; Amijima, Y.; Ibuki, K.; Hamanoue, K. *Rev. Sci. Instrum.* **1997**, *68*, 4364−4371.
(55) Capellos, C.; Bielski, B. H. J. *Kinetic Systems: Mathematical Description of Chemical Kinetics in Solution*; Wiley-Interscience: New York, 1972.
(56) Frisch, M. J.; Trucks, G. W.; Schlegel, H. B.; Scuseria, G. E.; Robb, M. A.; Cheeseman, J. R.; Scalmani, G.; Barone, V.; Mennucci, B.; Petersson, G. A.; Nakatsuji, H.; Caricato, M.; Li, X.; Hratchian, H. P.; Izmaylov, A. F.; Bloino, J.; Zheng, G.; Sonnenberg, J. L.; Hada, M.; Ehara, M.; Toyota, K.; Fukuda, R.; Hasegawa, J.; Ishida, M.; Nakajima, T.; Honda, Y.; Kitao, O.; Nakai, H.; Vreven, T.; Montgomery, J. A., Jr.; Peralta, J. E.; Ogliaro, F.; Bearpark, M.; Heyd, J. J.; Brothers, E.; Kudin, K. N.; Staroverov, V. N.; Kobayashi, R.; Normand, J.; Raghavachari, K.; Rendell, A.; Millam, J. M.; Klene, M.; Knox, J. E.; Cross, J. B.; Bakken, V.; Adamo, C.; Jaramillo, J.; Gomperts, R.; Stratmann, R. E.; Yazyev, O.; Austin, A. J.; Cammi, R.; Pomelli, C.; Ochterski, J.; Martin, R. L.; Morokuma, K.; Zakrzewski, V. G.; Voth, G. A.; Salvador, P.; Dannenberg, J. J.; Dappich, S.; Daniels, A. D.; Farkas, O.; Foresman, J. B.; Ortiz, J. V.; Cioslowski, J.; Fox, D. J.; *Gaussian 09* Revision A.01; Gaussian, Inc.: Wallingford, CT, 2009.
(57) Adamo, C.; Barone, V. *J. Chem. Phys.* **1999**, *110*, 6158−6170.
(58) Hay, P. J.; Wadt, W. R. *J. Chem. Phys.* **1985**, *82*, 270−283. Hay, P. J.; Wadt, W. R. *J. Chem. Phys.* **1985**, *82*, 284−298. Hay, P. J.; Wadt, W. R. *J. Chem. Phys.* **1985**, *82*, 299−310.
(59) Barone, V.; Cossi, M.; Tomasi, J. *J. Chem. Phys.* **1997**, *107*, 3210−3221.
(60) Cancès, E.; Mennucci, B.; Tomasi, J. *J. Chem. Phys.* **1997**, *107*, 3032−3041.